

Study of the Geothermal Potential of the Locality of Kaladi and Its Surroundings (Adamawa-Cameroon) from the Frequency Processing of Magnetic Data

Ndam Njikam Mohamed Moustapha^{1*}, Meying Arsène¹, Zanga Amougou Alain², Abdou Raouf³, Nkemndem Agendia Demianus⁴

¹School of Geology and Mining Engineering, University of Ngaoundere, Ngaoundere, Cameroon

²Department of Physics, Faculty of Sciences, University of Douala, Douala, Cameroon

³Research Center for Deep Ocean Science and Underwater Engineering, School of Resources and Geosciences, China University of Mining and Technology (CUMT), Xuzhou, China

⁴Department of Geography, University of Buea, Buea, Cameroon

Email: *ndamnjikamm@gmail.com

How to cite this paper: Moustapha, N.N.M., Arsène, M., Alain, Z.A., Raouf, A. and Demianus, N.A. (2022) Study of the Geothermal Potential of the Locality of Kaladi and Its Surroundings (Adamawa-Cameroon) from the Frequency Processing of Magnetic Data. *International Journal of Geosciences*, 13, 1024-1039.

<https://doi.org/10.4236/ijg.2022.1311052>

Received: October 7, 2022

Accepted: November 14, 2022

Published: November 17, 2022

Copyright © 2022 by author(s) and Scientific Research Publishing Inc. This work is licensed under the Creative Commons Attribution International License (CC BY 4.0).

<http://creativecommons.org/licenses/by/4.0/>



Open Access

Abstract

The aim of this study is to estimate the variations in curie point depth, geothermal gradient and heat flux from the frequency analysis of magnetic data in order to evaluate the geothermal potential of the Kaladi locality and its surroundings. For this purpose, the magnetic field map was first reduced to equator (RTE). The centroid method was used to divide the RTE grid into a set of 40 blocks. The spectral analysis applied to each block allowed determining the depth to top (Z_t), center (Z_0) and bottom (Z_b , also called curie point depth or CPD) of the magnetic sources. Knowing the different CPD, the geothermal gradient associated with each block was calculated. The heat flow was then calculated from the geothermal gradient associated with the anomaly block considered. From the set of values obtained for each block, maps of geothermal gradient and heat flow variations were established. Analysis of these maps shows that the sectors that could be favourable for geothermal exploration are the north of Kaladi and the Goro-Bembara corridor, because they show variations in the geothermal gradient and heat flow between 0.4 and 0.8°C/m and between 1.2 and 2 mW/m² respectively. In addition, the superposition of the different hot springs highlighted in previous studies with areas of high geothermal gradient and heat flow values supports this analysis. The proposed models can be used as background documents for any geothermal exploration project in the study area.

Keywords

Spectral Analysis, Curie Point Depth, Heat Flow, Geothermal Gradient

1. Introduction

Energy is the basis of any idea of industrialisation and is therefore one of the essential factors for socio-economic development. This is even truer for developed or industrialised countries than for developing countries like Cameroon (Central Africa). As far as Cameroon is concerned, the country has many sources of renewable energy such as biomass, wind, solar and geothermal energy, which remain largely untapped for a country that aspires to emerge. The area investigated in this study is located in the Adamawa, Cameroon region. It is bounded by longitudes 13°45' - 14°15' East and latitudes 06°00' - 06°45' North and covers an area of 5100 km². According to several previous studies ([1]-[7]), the geological setting of the Adamawa region seems to be favourable for the study of geothermal resources. Indeed, most geodynamic events such as volcanism, earthquakes, and the formation of mountain ranges associated with tectonic plate movements are controlled at the levels of the earth's crust by heat transfer. All these geodynamic phenomena are common to the Adamawa region and the study area in particular ([1] [8] [9] [10] [11] [12]). On a local scale, the compilation of previous studies shows that the study area lies within the central Cameroon shear Zone (CCSZ), which is a system of strike-slip faults within which the directions vary from N30°E to N70°E. This tectonic corridor, originally sinistral, was reactivated into a dextral shear during the late Pan-African evolution ([3] [4] [13] [14]), thus showing its instability. The development of this corridor would have taken place under high temperatures and pressures which would have caused a significant variation in the geothermal gradient in the area. This hypothesis is supported by the existence of numerous hot springs in the study area, which has been highlighted in previous studies ([5] [15]). These hot springs can therefore be associated with the magmatic processes generated by this tectonic corridor and the proximity of a volcanic system to the north of the study area (Figure 2). The structural model proposed by Ngako *et al.* [4] (Figure 1), shows the complexity and structural instability of the CCSZ. The major geological structures developed in this corridor at the scale of the study area may therefore correspond to areas of significant variation in the geothermal gradient. Since these structures can be interpreted from the contrast of magnetic susceptibilities, the magnetic method can be used to explore potential geothermal energy targets in the study area through the estimation of curie point depths as well as the calculation of the geothermal gradient and heat flow. This is the objective of this study.

2. Tectonic and Geological Setting

The compilation of the results of previous studies shows that the study area is

located in the central Cameroon shear zone (CCSZ) ([4] [6] [15] [16] [17]). This zone is a sub-domain of the central Cameroon domain (Figure 1), that is characterised by large strike-slip faults such as the CCSZ ([13]). This corridor constitutes a fault system within which the directions vary from N30°E to N70°E (Figure 1). According to Tchoua [18] et Kamgang [19], these directions correspond to those of the major Pan-African structures in North Cameroon. According to these authors, the N30°E direction of Ngaoundere coincides with that of the Cameroon volcanic line, while the N70°E direction corresponds to that of the Adamawa volcanic massif. Many studies have defined the CCSZ and its extension as dextral shear zones ([10] [16] [20] [21]). However, recent studies ([2] [4] [6] [13]) have revealed a sinistral shear superimposed on the posterior dextral shear in the same direction. According to Njonfang *et al.* [2], this superposition is because of the interference of two shear phases with opposite dip direction and similar direction, evolving successively under deep and superficial conditions, respectively. Structural studies of the Adamawa domain highlight four deformation phases: D1, D2, D3 et D4 ([3] [4] [13] [16] [22]). The D1 phase is marked by flat foliation associated with isoclinal folds and stretching lineations. The CCSZ was associated with the D2 phase ([2] [3] [13]), which was characterised by the formation of a pre-sinistral main shear. D2 was reactivated into a dextral shear at phase D3 during the late Pan-African evolution ([3] [4] [13] [16]).

According to the compilation of the studies of Toteu *et al.* [5] and Lasserre *et al.* [15], the study area covers the four main petrographic types (Figure 2), namely: sedimentary formations (sandstones, conglomerates, sands, etc.), volcanic formations (basalts, rhyolites, etc.), metamorphic formations (gneiss,

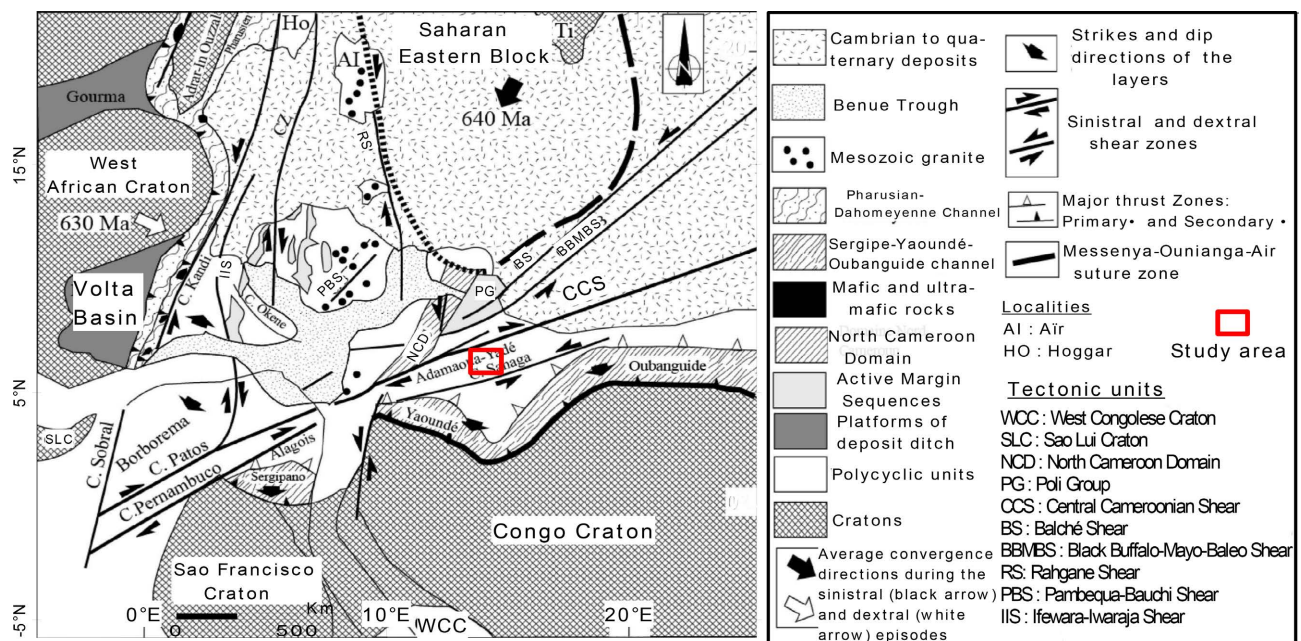


Figure 1. Kinematic evolution of the Pan-African-Brazilian chain, from Ngako *et al.* [4], modified. The dip directions of the second tectonic episode (black arrows) and the third tectonic episode (white arrows) in the North-Cameroonian domain.

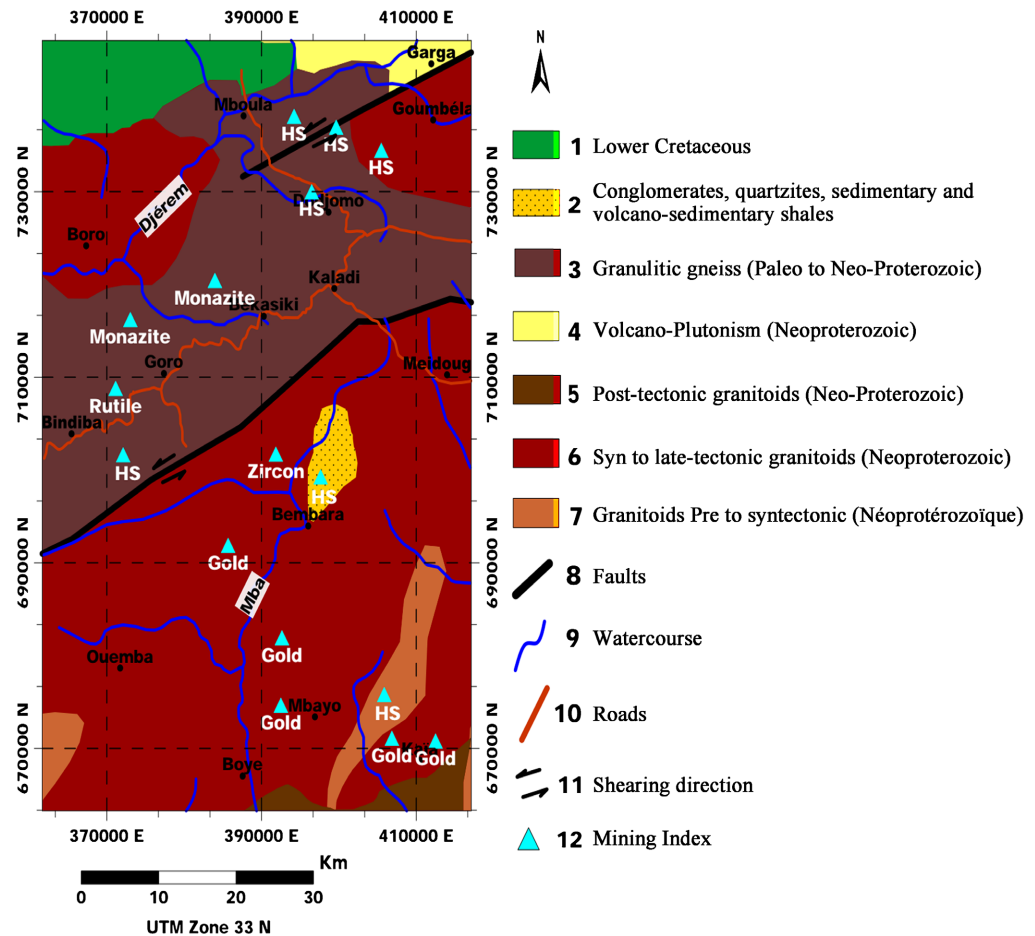


Figure 2. Geological map of the study area, according to Toteu *et al.* [5] and Lasserre *et al.* [15].

amphibolites, etc.) and plutonic formations (granites). The geological model proposed by these authors (**Figure 2**), shows a preferential orientation of the geological bodies (WSW-ENE) and the granito-gneissic nature of the basement of the study area. The model also highlights various mining index including: monazite, rutile, zircon, gold and several hot springs (HS). Thus, the location of the study area in a tectonic corridor (**Figure 1**), the presence of numerous hot springs highlighted by previous studies (**Figure 2**), the existence of volcanic formations (mainly to the north of the study area) and the structural instability linked to numerous phases of tectonic deformation, constitute a set of factors that could encourage geothermal exploration in the study area.

3. Data and Method

3.1. Origin of the Magnetic Data

The magnetic data used in this study were recorded during aeromagnetic surveys conducted between 1970 and 1976 by SURVAIR, on behalf of the Canadian International Development Agency. The aeromagnetic survey was conducted at a flight altitude of 235 m following N135°E directional profiles spaced 750 m apart, with a magnetometer of recording sensitivity ± 0.5 nT ([23]). Several cor-

rections were applied to the measured field data grid. We obtained the total magnetic intensity map (TMI) using the difference between the measured field and the fraction of the regional field or IGRF (International Geomagnetic Reference Field) for the date of 1 January 1970 and the minimum curvature as the interpolation method for a sampling step of 500 m (**Figure 3(A)**). A reduction equator filter (RTE) was applied to the TMI grid to bring the observed anomalies vertically over their respective causative sources. This was done by selecting a point at the center of the magnetic anomaly map (13.98°E and 06.38°N), with an inclination (I) and declination (D) of -10.41° and -4.82° , respectively, taken from the IGRF theoretical field model as of 1 January 1970. **Figure 3(B)** shows the resulting RTE map.

3.2. Method

3.2.1. Spectral Analysis

Spectral analysis has been widely used by several authors ([24]-[29]) for depth determination of magnetic and gravity anomalies. Since the gravity and magnetic anomalies can be conveniently treated as space series amenable to Fourier analysis and synthesis ([26] [27]), without in any way affecting the intrinsic features of these anomalies, spectral methods provide a powerful approach to their analysis and interpretation. Spectral analysis does not require knowledge of the geometry, the density contrast or magnetic susceptibility of the causative bodies; it simply asks the study of power or energy spectrum as a function of wavelength or frequency. The power or energy spectrum of the anomaly will have dominant high frequency components when the anomaly is continued to the proximity of the source ([26] [27]). The near-surface sources will thus give flatter, and the deeper sources will give steeper, power spectrum ([26] [27]). The depth (h) of an interface can be obtained by using the Gerard and Griveau [30] formula which is given below:

$$h = \Delta(\log E) / 4\pi\Delta(n) \quad (1)$$

where E represents the energy spectrum; $\Delta(\log E)$ is the variation of logarithm of energy spectrum in the interval of frequency $\Delta(n)$.

3.2.2. Curie Point Depth or CPD

The spectral analysis method is generally used to determine the curie point depth at a given point or CPD ([31]-[36]). The calculation of the CPD using the spectral analysis method can be done in the following four steps:

- Apply the centroid method to the magnetic grid reduced to the equator. This method consists of cutting the magnetic field grid into a set of square or rectangular blocks so that the central point of one block is one of the vertices of another block. The central point of each block is called “centroid”. The analysis of the power spectrum will make it possible to determine at this central point (on the vertical plane), the depth to top Z_b , to middle Z_0 (also called the centroid depth), and the depth to bottom Z_b , also called curie point depth (CPD).

- Switch the data for each block from the spatial to the frequency domain and calculate the power spectrum associated with each.
- Analyse the resulting power spectrum and calculate the centroid depth Z_0 (in the low frequencies) and the top depth Z_t (in the high frequencies) using the formula of Gerard and Griveau [30] given in Equation (1).
- Calculate the CPD or depth to bottom Z_b using the following equation:

$$Z_b = 2Z_0 - Z_t \quad (2)$$

3.2.3. Geothermal Gradient ($gradT$)

The geothermal gradient is defined as the observed increase in temperature of the subsurface as one moves away from the surface. The average earth gradient is $3^\circ\text{C}/100\text{m}$, but it can vary greatly depending on the geographical location ([37] [38]). Expressed in $^\circ\text{C}/\text{m}$ in this study, it is related to the CPD or Z_b and is calculated using the following formula:

$$gradT = \frac{dT}{dZ} = \frac{T_c - T_{sur}}{Z_b - Z_{sur}} \text{ } ^\circ\text{C}/\text{m} \quad (3)$$

In other words, the geothermal gradient is the temperature variation (dT) over the depth variation (dZ). In the expression of the $gradT$:

- T_{sur} is the average surface temperature. But in numerous studies, it is always assumed that the average surface temperature is 0°C ([39] [40] [41]). Other authors use instead the average annual temperature of the area concerned ([42] [43]).
- T_c is the curie temperature, the approximate value of which is defined by numerous authors as 580°C ([36] [41] [43]);
- Z_b is the curie point depth or CPD;
- Z_{sur} is the surface depth generally considered to be zero ($Z_{sur}=0$).

Considering $Z_{sur} = 0$ and $T_{sur} = 0$, the expression of the geothermal gradient becomes:

$$gradT = \frac{dT}{dZ} = \frac{T_c}{Z_b} \text{ } ^\circ\text{C}/\text{m} \quad (4)$$

3.2.4. Heat Flow (Q_z)

Considering $Z_{sur} = 0$ and $T_{sur} = 0$, the geothermal gradient is then related to the heat flow by the following equation:

$$Q_z = C_i \frac{dT}{dZ} = C_i \frac{T_c}{Z_b} \text{ mW}/\text{m}^2 \quad (5)$$

where C_i is the thermal conductivity (the amount of heat in watts transferred through a square or rectangular area of material of given thickness due to a temperature difference). A thermal conductivity of $2.5 \text{ Wm}^{-1} \cdot ^\circ\text{C}^{-1}$ is considered average for igneous rocks ([36] [44] [45]).

It is important to know that for geothermal exploration, areas with high values of geothermal gradient or heat flow are generally sought.

4. Results and Discussion

The Total Magnetic Intensity or TMI map (Figure 3(A)) was produced using the “Minimum curvature” as the interpolation method for a sampling step of 500 m (related to the spacing of the measurement points). In order to bring the observed anomalies vertically to the causative sources, the TMI grid has been reduced to equator (RTE) using the parameters described in the methodology. The resulting RTE grid (Figure 3(B)) shows important positive and negative anomalies of different shapes, orientations and intensities that probably reflect a variation in the depths of the magnetic sources:

- Positive anomalies (with intensities between 18 and 381 nT) are observed at the North (north of Mboula), at the Centre (along the corridor from Bindiba to Kaladi) and at the South (along the corridor from Boye to Kaia). The large positive anomaly situated at the north of Mboula does not appear entirely within the study area due to the limitations of the dataset used; but if it is to be characterised within the area, it can be said to be roughly circular and elongated (oval) with an E-W orientation. The positive anomalies along the Bindiba-Kaladi path (in the centre), which are much straighter, therefore belong to the same corridor with an approximate ENE-WSW direction. The Boye-Kaia anomalies, very elongated and less circular than the north of

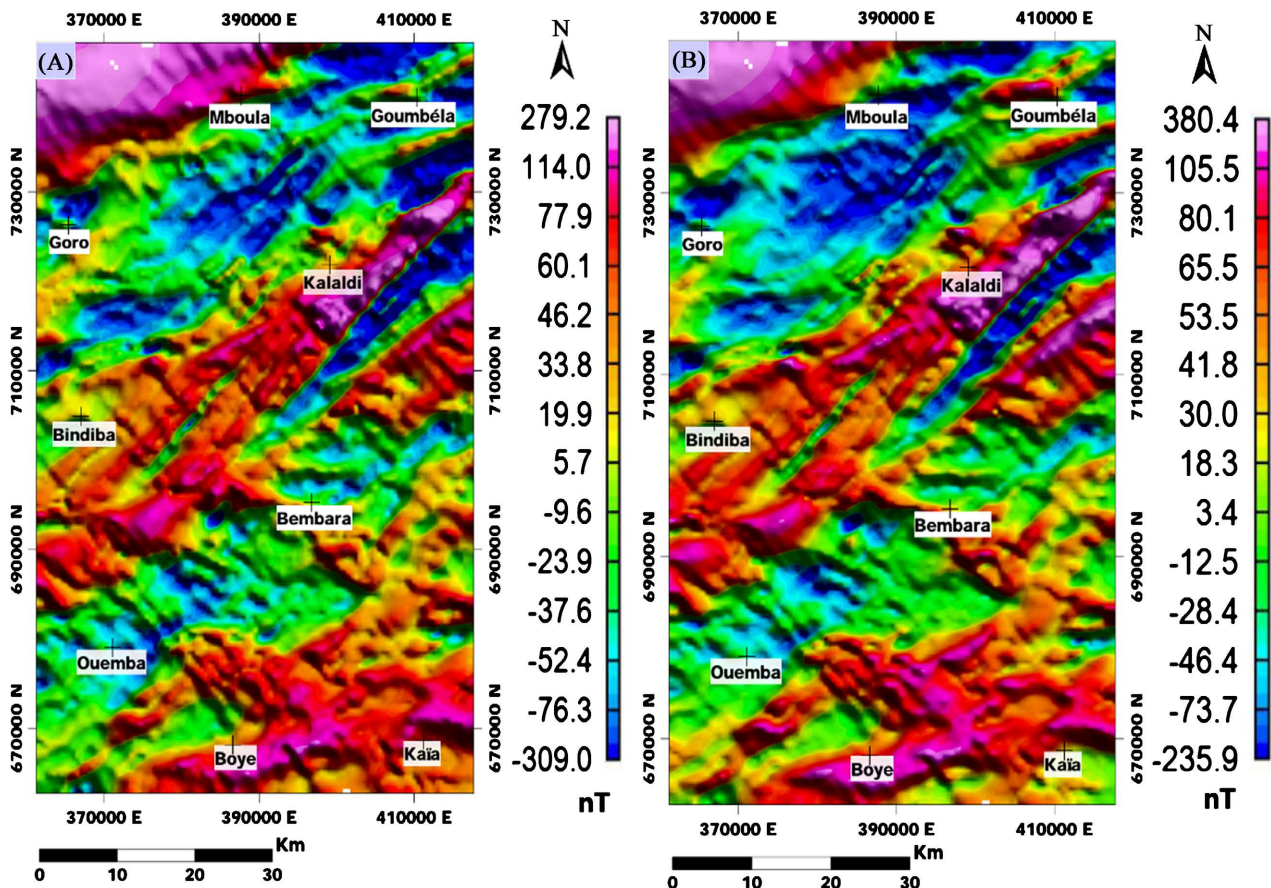


Figure 3. TMI map (A); RTE map (B).

Mboula, also have an E-W direction. We thus find ourselves in a configuration where we have two more or less parallel corridors of E-W anomalies, linked together by a diagonal corridor of ENE-WSW anomalies. This configuration is common to the strike-slip zone.

- The negative anomalies (with intensities between -236 and -12 nT) occupy two large anomaly corridors with a NE-SW direction: the Goro-Mboula-Goumbéla anomaly corridor and the Ouemba-Bembara corridor. A detailed analysis of the RTE shows that each of the two negative anomaly corridors is bounded by two positive anomaly corridors (the Goro-Mboula-Goumbéla corridor lies between the large positive anomaly at the north of Mboula and that of the Bindiba-Kaladi corridor, while the Ouemba-Bembara corridor lies between the Bindiba-Kaladi corridor and that of Boye-Kaïa). These anomalies are specific to diamagnetic bodies which are characterised by a lack of remanence. This alternation of positive and negative anomalies thus shows the existence of horst-graben structures in the study area.

In order to study the depths of the magnetic sources and thus calculate the different CPD, the centroid method was first applied to the RTE grid. It consisted in cutting the RTE grid into a set of 40 rectangular blocks of dimensions $14 \text{ km} \times 17 \text{ km}$ (Figure 4(A)). The magnetic data associated with each of the

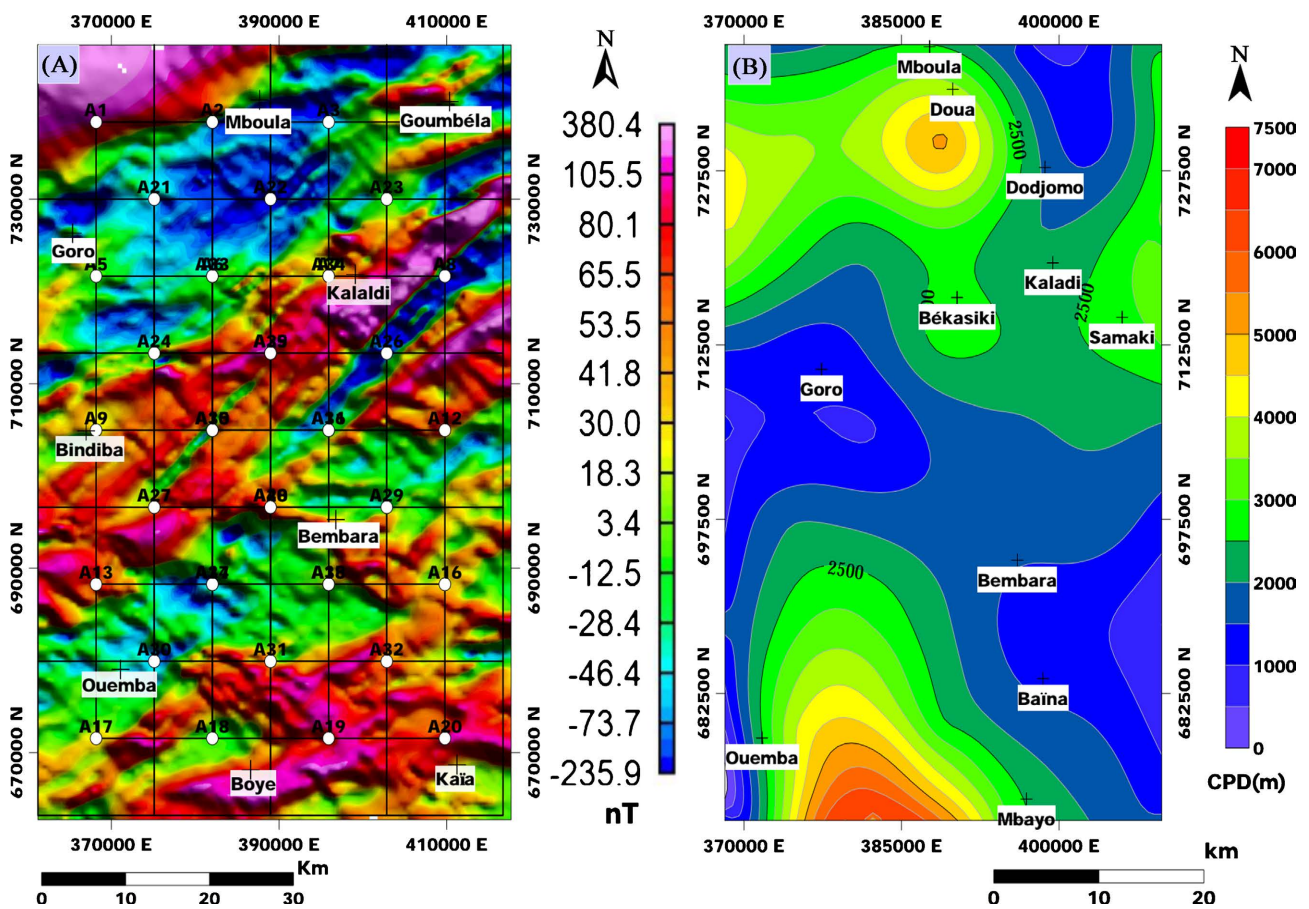


Figure 4. (A) Map of the different anomaly blocks; (B) Map of the curie point depth.

anomaly blocks in the spatial domain were all transformed into frequency data. The transformation from the spatial to the frequency domain was then used to develop a set of power spectra associated with each of the 40 blocks (Figure 5). The analysis of each spectrum allows us to understand its variation and thus to identify the spectral domains in which the parameters Z_0 and Z_t will be calculated on the vertical plane. Z_0 corresponds to the depth at the center and is calculated in the low frequency domain (Figure 5). Z_t is the depth to the top and is calculated in the high frequency domain (Figure 5). In each of these domains (low and high frequencies), the Z_0 and Z_t parameters of each of the 40 blocks were evaluated using the formula of Gerard and Griveau [30] given by Equation (1). Knowing these two parameters, the different CPD or Z_b could be calculated using Equation (2). All the CPD values for the 40 blocks are given in Table 1. The interpolation of all these depths according to the minimum curvature method led to the elaboration of the map of curie point depth (Figure 4(B)). This map shows a variation in depth from the surface to a maximum of 7500 m, with maximum depths mainly located in the south and north of the study area (Figure 4(B)).

Knowing the different CPD, the geothermal gradient (gradT) associated with each centroid was calculated. This was done by taking the temperature and depth at the surface to be equal to zero as given by equation 4 ($Z_{sur} = 0$ et $T_{sur} = 0$). All these calculation results are recorded in Table 1 and their interpolation according to the minimum curvature method made it possible to elaborate the map of the geothermal gradient variations of the study area (Figure 6(A)). This map shows that the areas with high geothermal gradient values are mainly located at the north of Kaladi and along the Goro-Bembara corridor with a gradient variation between $0.4^\circ\text{C}/\text{m}$ and $0.8^\circ\text{C}/\text{m}$. From the geothermal gradient, the heat flow (Q_z) associated with each centroid was also calculated using Equation (5). All these calculation results are shown in Table 1. As before, the heat flow variation map (Figure 6(B)) was obtained by interpolation of all the results obtained. As in the case of the geothermal gradient, this map shows a significant variation in heat flow at the north of Kaladi and along the Goro-Bembara corridor with values between 1.2 et $2 \text{ mW}/\text{m}^2$.

Based on the analysis of the geothermal gradient and heat flow maps, it is clear that the sectors of the study area that could be favourable for geothermal exploration are the north of Kaladi and the Goro-Bembara corridor respectively. This is because these sectors present significant variations in geothermal gradient and heat flow between $0.4^\circ\text{C}/\text{m}$ and $0.8^\circ\text{C}/\text{m}$ and between 1.2 and $2 \text{ mW}/\text{m}^2$ respectively. Also, if we superimpose all the mining index resulting from the compilation of the studies of Toteu *et al.*, 2008 [5] and Lasserre *et al.*, 1961 [15] (Figure 2) on the geothermal gradient and heat flow maps respectively, we can see that the different hot springs identified by these authors are located in areas with high geothermal gradient and heat flow values. The location of these favourable sectors can be justified by the existence of volcanic formations to the north of

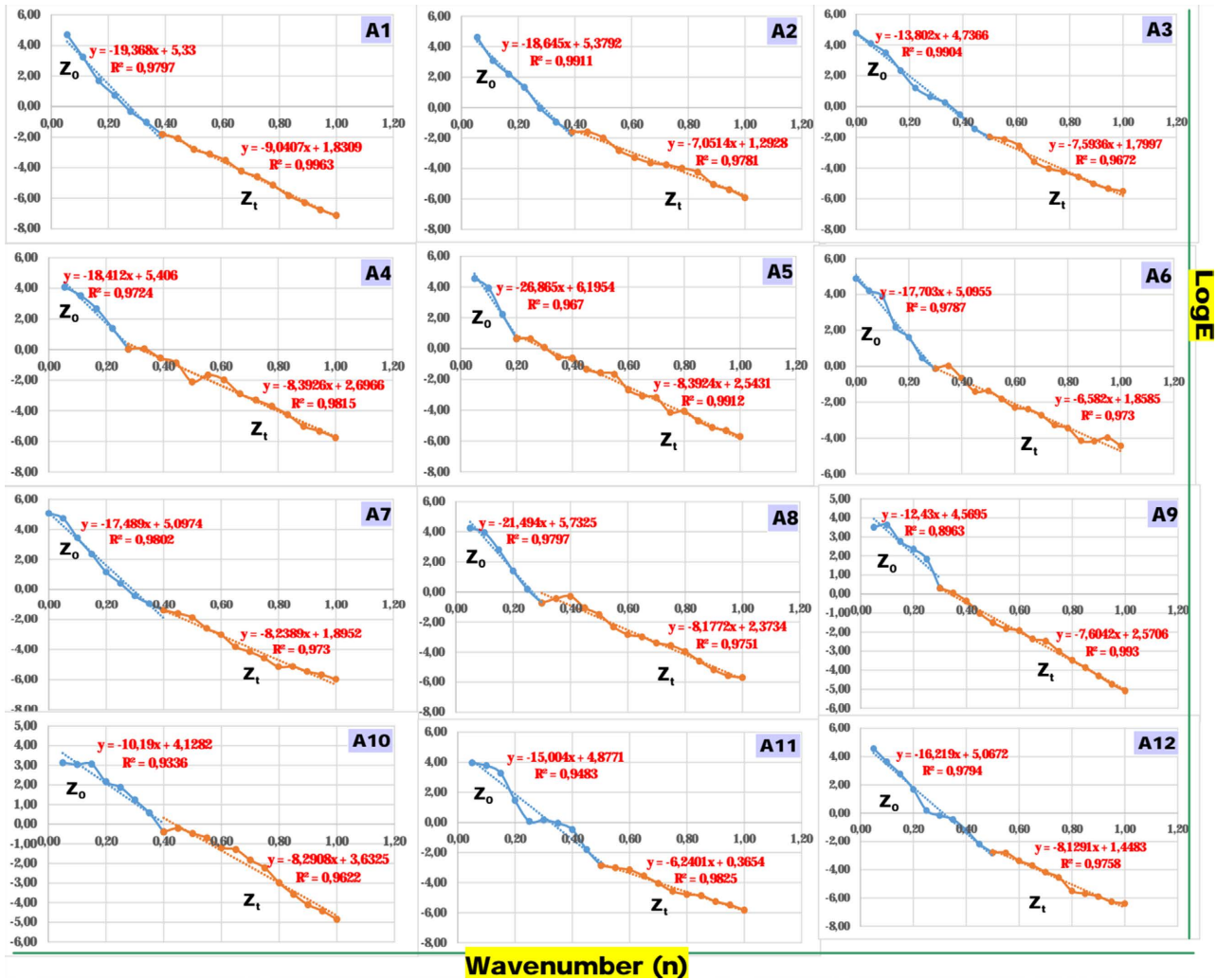


Figure 5. Power spectrum associated with the first 12 anomaly blocks.

Table 1. Summary of the different parameters calculated for the 40 blocks.

Easting (m)	Northing (m)	CDP (m)	$gradT$ ($^{\circ}C/m$)	Q_z (mW/m^2)	Block
368183.512	738354.332	2364.27548	0.24531828	0.61329571	A1
382050.27	738354.332	2407.53185	0.24091062	0.60227656	A2
395917.027	738354.332	1592.86624	0.36412348	0.9103087	A3
409783.785	738354.332	2263.6465	0.25622375	0.64055938	A4
368183.512	721657.032	3609.68153	0.16067899	0.40169749	A5
382050.27	721657.032	2294.90446	0.25273383	0.63183458	A6
395917.027	721657.032	2128.90924	0.27243998	0.68109996	A7
409783.785	721657.032	2771.56051	0.20926839	0.52317097	A8
368183.512	704959.733	1373.86943	0.4221653	1.05541325	A9
382050.27	704959.733	962.515924	0.60258743	1.50646858	A10
395917.027	704959.733	1892.34873	0.30649742	0.76624355	A11

Continued

409783.785	704959.733	1935.42197	0.29967625	0.74919063	A12
368183.512	688262.434	1790.91561	0.32385669	0.80964173	A13
382050.27	688262.434	3348.21656	0.17322655	0.43306637	A14
395917.027	688262.434	1450.44586	0.39987704	0.9996926	A15
409783.785	688262.434	1015.92357	0.57090909	1.42727273	A16
368183.512	671565.135	1509.87261	0.38413837	0.96034592	A17
382050.27	671565.135	5196.15446	0.11162101	0.27905252	A18
395917.027	671565.135	2548.55892	0.22757959	0.56894898	A19
409783.785	671565.135	1630.02389	0.35582301	0.88955752	A20
375116.73	730005.876	3538.97293	0.16388936	0.40972339	A21
388983.166	730005.876	5065.55732	0.11449875	0.28624688	A22
402849.601	730005.876	1248.92516	0.46439932	1.16099831	A23
375116.73	713308.964	1429.90446	0.40562151	1.01405377	A24
388983.166	713308.964	2678.44745	0.21654336	0.54135839	A25
402849.601	713308.964	2544.75318	0.22791994	0.56979986	A26
375116.73	696612.053	2081.64013	0.27862645	0.69656613	A27
388983.166	696612.053	1733.08917	0.33466253	0.83665631	A28
402849.601	696612.053	1733.8535	0.334515	0.83628749	A29
375116.73	679915.142	3943.51115	0.14707705	0.36769263	A30
388983.166	679915.142	2616.44904	0.22167449	0.55418622	A31
402849.601	679915.142	1517.61943	0.3821775	0.95544375	A32
382049.795	721657.604	2241.19427	0.2587906	0.64697649	A33
395915.925	721657.604	2115.65287	0.27414705	0.68536763	A34
382049.795	704961.061	992.969745	0.58410642	1.46026604	A35
395915.925	704961.061	1892.34873	0.30649742	0.76624355	A36
382049.795	688264.517	2598.18471	0.22323278	0.55808195	A37
395915.925	688264.517	1271.67197	0.45609246	1.14023115	A38
388982.716	713309.506	2683.28822	0.2161527	0.54038176	A39
388982.716	696613.311	1755.89172	0.3303165	0.82579124	A40

the study area and the tectonic context in which the study area is located. This proves that the study area is potentially rich in geothermal energy, particularly in the sectors mentioned above. The models proposed in this study can therefore be used for more detailed geothermal exploration of the study area.

5. Conclusion

The aim of this study, based on the processing of magnetic data, was to analyze the

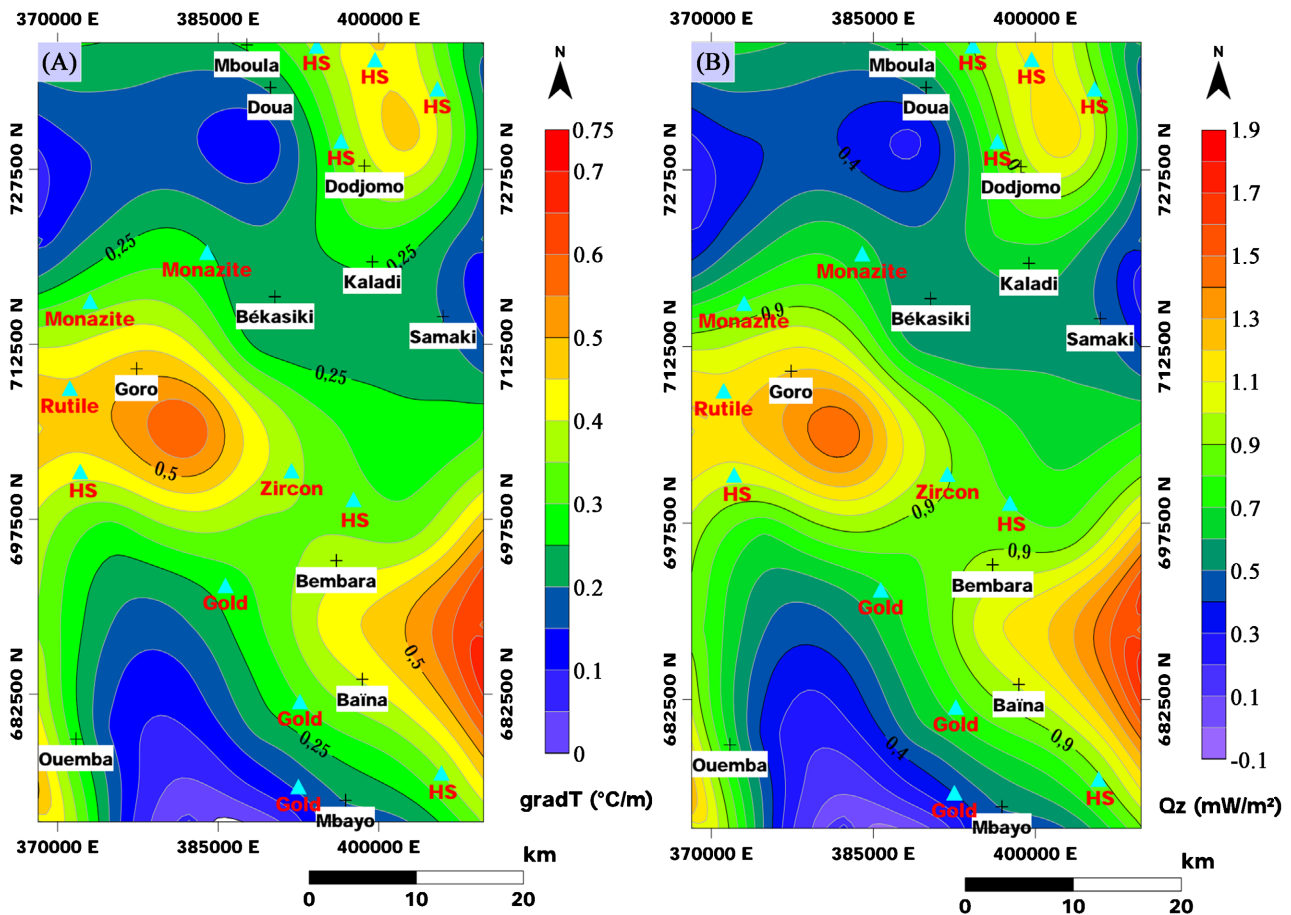


Figure 6. (A) Map of geothermal gradient variations; (B) Map of heat flow variations; The small coloured triangles correspond to the distribution of mining index taken from the compilation of studies carried out by Toteu *et al.*, 2008 [5] and Lasserre *et al.*, 1961 [15].

geothermal potential of the Kaladi locality and its surroundings. This objective was achieved by following a very specific methodology to calculate a set of parameters (curie point depth, geothermal gradient and heat flow) from the frequency processing of the magnetic data. First, the magnetic field grid was reduced to equator in order to bring the anomalies vertically to the causative sources. Using the centroid method, the RTE grid was split into a set of 40 rectangular blocks. Each of the block databases was transformed into a frequency database and a set of power spectra was developed. The analysis of each spectrum allowed the determination of the depths to center Z_0 , to top Z_t and the curie point depth (CPD) or Z_b associated with each block. Knowing the different CPD, the geothermal gradient associated with each block was calculated. The heat flow for each block was then calculated from the value of the geothermal gradient associated with the block. Using all the calculated geothermal gradient and heat flow values, maps of geothermal gradient and heat flow variations were developed. The analysis of these maps shows that the sectors that could be favourable for geothermal exploration are respectively the north of Kaladi and the Goro-Bembara corridor, as they present significant geothermal gradient and heat flux variations of between

0.4°C/m and 0.8°C/m and between 1.2 and 2 mW/m² respectively. This last conclusion is confirmed by the fact that the various hot springs identified by previous studies overlap perfectly with the areas of high geothermal gradient and heat flow. The models proposed in this study can therefore be used as background document for any geothermal exploration project in the study area.

Acknowledgements

The authors are grateful to Professor ABDOUL WAHABOU, Director of School of Geology and Mining Engineering, University of Ngaoundere, for providing the infrastructural facilities. We are also thankful to those people who help in different stages of this work.

Disclosure Statement

No potential conflict of interest was reported by the authors.

Conflicts of Interest

The authors declare no conflicts of interest regarding the publication of this paper.

References

- [1] Gaudru, H. and Tchouankoue, J.P. (2002) The 1999 Eruption of Mount Cameroon, West Africa. *Cogeoenvironment Newsletters*, **18**, 12-14.
- [2] Njonfang, E., Ngako, V., Kwékam, M. and Affaton, P. (2006) Les orthogneiss calco-alcalins de Foumban-Bankim: Témoins d'une zone interne de marge active panafricaine en cisaillement. *Comptes Rendus Geoscience*, **338**, 606-616. <https://doi.org/10.1016/j.crte.2006.03.016>
- [3] Tchameni, R., Pouclet, A., Penaye, J., Ganwa, A.A. and Toteu, S.F. (2006) Petrography and Geochemistry of the Ngaoundéré Pan-African Granitoids in Central North Cameroon: Implications for Their Sources and Geological Setting. *Journal of African Earth Sciences*, **44**, 511-529. <https://doi.org/10.1016/j.jafrearsci.2005.11.017>
- [4] Ngako, V., Affaton, P. and Njonfang, E. (2008) Pan-African Tectonic in Northwestern Cameroon: Implication for History of Western Gondwana. *Gondwana Research*, **14**, 509-522. <https://doi.org/10.1016/j.gr.2008.02.002>
- [5] Toteu, S.F., Penaye, J., Deschamps, Y., Maldan, F., Nyama Atibagoua, B., Bouyou Houketchang, M., Sep Nlomgan, J.P. and Mbola Nzana, S.P. (2008) Géologie et ressources minérales du Cameroun. *33rd International Geological Congress*, Oslo, 6-14 August 2008.
- [6] Njanko, T., Nédelec, A., Kwékam, M., Siqueira, R. and Esteban, L. (2010) Emplacement and Deformation of the Fomopéa Pluton: Implication for the Pan-African History of Western Cameroon. *Journal of Structural Geology*, **32**, 306-320. <https://doi.org/10.1016/j.jsg.2009.12.007>
- [7] Tchouatcha, S.M., Njiké Ngaha, P.R., Salah, M.M., Deaf, A.S. and Ekodeck, E.G. (2010) Existence of "Late Continental" Deposits in the Mbere and Djerem Sedimentary Basins (North Cameroon): Palynologic and Stratigraphic Evidence. *Journal of Geology and Mining Research*, **2**, 159-169.
- [8] Dorbath, C. and Dorbath, L. (1984) Approche sismologique de la structure de la

lithosphère en Afrique de l'Ouest. Université Pierre et Marie Curie, Paris, 307 p.

- [9] Stuart, G.W., Fairhead, J.D., Dorbath, C. and Dorbath, L. (1985) A Seismic Refraction Study of the Crustal Structure Associated with the Adamawa Plateau and Garoua Rift, Cameroon, West Africa. *Geophysical Journal International*, **81**, 1-12. <https://doi.org/10.1111/j.1365-246X.1985.tb01346.x>
- [10] Dorbath, L., Dorbath, C., Fairhead, J. and Stuart, G. (1986) A Teleseismic Delay Time Study across the Central African Shear Zone in the Adamawa Region of Cameroon, West Africa. *Geophysical Journal International*, **86**, 751-766. <https://doi.org/10.1111/j.1365-246X.1986.tb00658.x>
- [11] Tabod, C. (1991) Seismological studies of the Cameroon Volcanic Line in West Africa. University of Leeds, Leeds, 278 p.
- [12] Tabod, C., Fairhead, J.D., Stuart, G.W., Ateba, B. and Ntepe, N. (1992) Seismicity of the Cameroon Volcanic Line, 1982-1990. *Tectonophysics*, **212**, 303-320. [https://doi.org/10.1016/0040-1951\(92\)90297-J](https://doi.org/10.1016/0040-1951(92)90297-J)
- [13] Ngako, V., Affaton, P., Nnange, J. and Njanko, T. (2003) Pan-African Tectonic Evolution in Central and Southern Cameroon: Transpression and Transtension during Sinistral Shear Movements. *Journal of African Earth Sciences*, **36**, 207-214. [https://doi.org/10.1016/S0899-5362\(03\)00023-X](https://doi.org/10.1016/S0899-5362(03)00023-X)
- [14] Toteu, S.F., Penaye, J. and Poudjom Djomani, Y. (2004) Geodynamic Evolution of the Pan-African Belt of Central Africa with Special Reference to Cameroon. *Canadian Journal of Earth Sciences*, **41**, 73-85. <https://doi.org/10.1139/e03-079>
- [15] Lassere, M. (1961) Carte géologique de reconnaissance à l'échelle 1/500 000 du territoire du Cameroun, Ngaoundéré Est. Dir, Mines Geol Cameroon, Yaoundé.
- [16] Ngako, V., Jegouzo, P. and Nzenti, J. (1991) Le Cisaillement Centre Camerounais. Rôle structural et géodynamique dans l'orogénèse panafricaine. *Comptes Rendus de l'Académie des Sciences*, **313**, 457-463.
- [17] Kamwa, A.N., Owona, S., Tchakounté, J. and Ondo, J.M. (2016) Fabriques en aplatissement et constriction des granitoïdes de Nga Mbappé et de Yoro au nord du Groupe de Yaoundé (CPNE, Cameroun): Témoins de la mise en place de granites syn-tectoniques au cours de l'orogénèse Pan-Africaine. *Comunicações Geológicas*, **103**, 5-16.
- [18] Tchoua, F.M. (1974) Contribution à l'étude géologique et pétrographique de quelques volcans de la ligne du Cameroun (monts Manengouba et Bambouto). Université Clermont-Ferrand, Clermont-Ferrand, 333 p.
- [19] Kamgang, P. (2003) Pétrologie et géochimie d'un secteur clé de la Ligne du Cameroun, les Monts Bamenda: implications sur la genèse et l'évolution des magmas. Université de Yaoundé I, Yaoundé, 372 p.
- [20] Rolin, P. (1995) La zone de décrochements panafricains des Oubanguides en République Centrafricaine. *Comptes Rendus de l'Académie des Sciences (Paris)*, **320**, 63-69.
- [21] Nzenti, J.P., Kapajika, B., Wörner, G. and Lubala, T.R. (2006) Synkinematic Emplacement of Granitoids in a Pan-African Shear Zone in Central Cameroon. *Journal of African Earth Sciences*, **45**, 74-86. <https://doi.org/10.1016/j.jafrearsci.2006.01.005>
- [22] Ganwa, A.A., Frisch, W., Siebel, W., Shang, C.K., Ondo, J.M., Satir, M. and Numbem, J.T. (2008) Zircon $^{207}\text{Pb}/^{206}\text{Pb}$ Evaporation Ages of Panafrican Metasedimentary Rocks in the Kombé-II Area (Bafia Group, Cameroon): Constraints on Protolith Age and Provenance. *Journal of African Earth Sciences*, **51**, 77-88. <https://doi.org/10.1016/j.jafrearsci.2007.12.003>

- [23] Paterson, G. and Ltd, W. (1976) Interpretation of an Aeromagnetic Survey Overpart of the United Republic of Cameroon. ACDI Toronto, Toronto, 190 p.
- [24] Spector, A. and Grant, F. (1970) Statistical Models for Interpreting Aeromagnetic data. *Geophysics*, **35**, 293-302. <https://doi.org/10.1190/1.1440092>
- [25] Gerard, A. and Debeglia, N. (1975) Automatic Three-Dimensional Modeling for the Interpretation of Gravity or Magnetic Anomalies. *Geophysics*, **40**, 1014-1034. <https://doi.org/10.1190/1.1440578>
- [26] Pal, P., Khurana, K. and Unnikrishnan, P. (1979) Two Examples of Spectral Approach to Source Depth Estimation in Gravity and Magnetic. *Pure and Applied Geophysics*, **117**, 772-783. <https://doi.org/10.1007/BF00879978>
- [27] Reeves, C. (2005) Aeromagnetic Surveys: Principles, Practice and Interpretation. Earth-Works, Washington DC, 155 p.
- [28] Nguimbous-Kouoh, J.J., Ndougsa-Mbarga, T. Njandjock-Nouck, P., Eyike, A., Campos-Enríquez, J.O. and Manguelle-Dicoum, E. (2010) The Structure of the Goulfey-Tourba Sedimentary Basin (Chad-Cameroon): A Gravity Study. *Geofísica Internacional*, **49**, 181-193. <https://doi.org/10.22201/igeof.00167169p.2010.49.4.127>
- [29] Abate Essi, J.M., Marcel, J., Diab, A.D., Yene Atangana, J.Q., Monique, A.A. and Joseph Mvondo, O. (2019) Gravity Modeling of the Au-U Mineralized Crust at the North-Central Cameroon Illustrating Crustal Permeability. *Natural Resources Research*, **29**, 473-497. <https://doi.org/10.1007/s11053-019-09506-4>
- [30] Gerard, A. and Griveau, P. (1972) Quantitative Interpretation of Gravity or Magnetic Fields from Transformed Maps of the Fields' First Vertical Derivative. *Geophysical Prospecting*, **20**, 459-481. <https://doi.org/10.1111/j.1365-2478.1972.tb00648.x>
- [31] Okubo, Y., Graf, J.R., Hansen, R.O., Ogawa, K. and Tsu, H. (1985) Curie Point Depths of the Island of Kyushu and Surrounding Areas Japan. *Geophysics*, **50**, 481-494. <https://doi.org/10.1190/1.1441926>
- [32] Blakely, R.J. (1988) Curie Temperature Isotherm Analysis and Tectonic Implications of Aeromagnetic Data from Nevada. *Journal of Geophysical Research: Solid Earth*, **93**, 11817-11832. <https://doi.org/10.1029/JB093iB10p11817>
- [33] Tsokas, G.N., Hansen, R.O. and Fytikas, M. (1998) Curie Point Depth of the Island of Crete (Greece). *Pure and Applied Geophysics*, **152**, 747-757. <https://doi.org/10.1007/s000240050175>
- [34] Dolmaz, M.N., Hisarli, Z.M., Ustaömer, T. and Orbay, N. (2005) Curie Point Depths Based on Spectrum Analysis of Aeromagnetic Data, West Anatolian Extensional Province, Turkey. *Pure and Applied Geophysics*, **162**, 571-590. <https://doi.org/10.1007/s00024-004-2622-2>
- [35] Bilgin, O. (2018) The Importance of Geothermal Energy Resources in Turkey. *Open Access Library Journal*, **5**, Article ID: 82734. <https://doi.org/10.4236/oalib.1104317>
- [36] Njeudjang, K., Kana, J.D., Tom, A., Abate Essi, J.M., Djongyang, N. and Tchinda, R., (2020) Curie Point Depth and Heat Flow Deduced from Spectral Analysis of Magnetic Data over Adamawa Volcanic Region (Northern Cameroon): Geothermal Implications. *SN Applied Sciences*, **2**, Article No. 1330. <https://doi.org/10.1007/s42452-020-3099-z>
- [37] Eppelbaum, L., Kutasov, I. and Pilchin, A. (2014) Thermal Properties of Rocks and Density of Fluids. In: *Applied Geothermics. Lecture Notes in Earth System Sciences*. Springer, Berlin, 99-149. https://doi.org/10.1007/978-3-642-34023-9_2
- [38] Li, C., Yu, L. and Wang, J. (2017) A Global Reference Model of Curie-Point Depths

based on EMAG2. *Scientific Reports*, **7**, Article No. 45129.

<https://doi.org/10.1038/srep45129>

- [39] Tanaka, A., Okubo, Y. and Matsubayashi, O. (1999) Curie Point Depth Based on Spectrum Analysis of the Magnetic Anomaly Data in East and Southeast Asia. *Tectonophysics*, **306**, 461-470. [https://doi.org/10.1016/S0040-1951\(99\)00072-4](https://doi.org/10.1016/S0040-1951(99)00072-4)
- [40] Selim, E.I. and Aboud, E. (2014) Application of Spectral Analysis Technique on Ground Magnetic Data to Calculate the Curie Depth Point of the Eastern Shore of the Gulf of Suez, Egypt. *Arabian Journal of Geosciences*, **7**, 1749-1762. <https://doi.org/10.1007/s12517-013-0868-7>
- [41] Bilim, F., Akay, T., Aydemir, A. and Kosaroglu, S. (2016) Curie Point Depth, Heat-Flow and Radiogenic Heat Production Deduced from the Spectral Analysis of the Aeromagnetic Data for Geothermal Investigation on the Menderes Massif and the Aegean Region, Western Turkey. *Geothermics*, **60**, 44-57. <https://doi.org/10.1016/j.geothermics.2015.12.002>
- [42] Qingqing, Q., Qingsheng, L., Ning, Q., Yuanyuan, F., Sutaο, Z., Yao, W., Tao, Y. and Zhenmin, J. (2008) Investigation of Curie Point Depth in Sulu Ultra-high-Pressure Metamorphic Belt, Eastern China. *Journal of China University of Geosciences*, **19**, 282-291. [https://doi.org/10.1016/S1002-0705\(08\)60046-1](https://doi.org/10.1016/S1002-0705(08)60046-1)
- [43] Salem, A., Hussein, W., Ion, D., Bruno, P.S., Wu, S. and Borsato, R. (2017) Predicting Heat Flow and Determining Crustal Type Based on Integrated Interpretation of Seismic, Gravity and Magnetic Data in the Offshore Jazan Area, Southern Red Sea. *SPE Middle East Oil & Gas Show and Conference*, 6-9 March 2017, Manama. <https://doi.org/10.2118/183707-MS>
- [44] Maden, N. (2012) Geophysical Approach for the Detection and Evaluation of Geothermal Energy Potential Stimulated from Geology and Tectonics in Cappadocia Region (Central Turkey). In: Yang, J., Ed., *Geothermal Energy, Technology and Geology*, Nova Science, Hauppauge.
- [45] Speranza, F., Minelli, L., Pignatelli, A. and Gilardi, M. (2016) Curie Temperature Depths in the Alps and the Po Plain (Northern Italy): Comparison with Heat Flow and Seismic Tomography Data. *Journal of Geodynamics*, **98**, 19-30. <https://doi.org/10.1016/j.jog.2016.03.012>